Korean Journal of Remote Sensing, Vol.27, No.3, 2011, pp.339~351

Investigation of Urban Environmental Quality Using an Integration of Satellite, Ground based measurement data over Seoul, Korea

Kwon Ho Lee*†, Man Sing Wong and Young J. Kim*****

*Dept. of Satellite Geoinformatics Engineering, Kyungil University

**Dept. of Land Surveying and Geo-Informatics, The Hong Kong Polytechnic University, Kowloon, Hong Kong

***Advanced Environmental Monitoring Research Center (ADEMRC), Gwangju Institute of Science & Technology (GIST), Gwangju, Korea

Abstract : This study investigates the potentials of satellite, ground measurement data, and geo-spatial information within an urban area for the mapping of the Urban Environmental Quality (UEQ) parameters. The UEQ indicates a complex and various parameters resulting from both human and natural factors, which are greenness, climate, air pollution, the urban infrastructure, and etc. Multi-spectral remote sensing data from the Landsat ETM and TM sensors for the mapping of air pollution by the Haze Optimized Transform (HOT) technique, Urban Heat Island (UHI) using the emissivity-fusion method in Seoul from 2000 to 2006 in fine resolution (30m) were analyzed for the estimation of UEQ index. Although the UHI values are similar (8.4°C ~ 9.1°C) during these years, the spatial coverage of "hot" surface temperature (> 24°C) significantly increased from 2000 to 2006 due to the rapid urban development. Furthermore, high correlations between vegetation index and land surface temperature were achieved with a correlation coefficients of 0.85 (2000), 0.81 (2001), 0.84 (2002), and 0.89 (2006), respectively. It was found that the proposed method was successfully analyzed spatial structure of the UEQ and the scenarios of the best and worst areas within the city were also identified. Based on the quantifiable fine resolution satellite image parameters, UEQ can promote the understanding of the complex and dynamic factors controlling urban environment.

Key Words : Remote sensing, Urban heat island, Landsat, Urban environmental quality.

1. Introduction

In recent years, the integrated use of satellite remote sensing data and Geographic Information System (GIS) for urban studies has increasingly been made. This allows estimating the change detection and environmental impact classification and assessment in urban areas. Forster (1983) developed a residential quality index in the city of Sydney, Australia, using spectral reflectance data derived from

Received May 31, 2011; Revised June 18, 2011; Accepted June 19, 2011.

† Corresponding Author: Kwon Ho Lee (khlee@kiu.ac.kr)

Landsat MSS images. Weber and Hirsch (1992) measured the urban life quality of Strasbourg, France, by combining the high resolution SPOT image data with cartographic and census data. Lo and Faber (1997) demonstrated the usefulness of Landsat TM image in conjunction with census data for quality of life assessment in a small city in Georgia with emphasis on Normalized Difference Vegetation Index (NDVI) as a desirable quality indicator of urban morphological environment. Most recently, the spatial structure of the thermal urban environment in major cities have been conducted using thermal images from high resolution satellite data (Voogt and Oke, 2003; Nichol and Wong, 2005; Stathopoulou and Cartalis, 2007).

The urban environment is an important concern in quality of human life. Because it is related with various sociological items, single definition or method is difficult to measure especially in complex urban environment. What is clear from the recent literature is that the Urban Environmental Quality (UEQ), as a consensual objective indicator, is able to be determined by reliable information based on would it be better to change to: biogeophysical, geomorphological and dynamic processes, as well as climate change effects. The Urban Heat Island (UHI), the distribution of greenery, building density, and air quality are affecting factors on UEQ (Nichol *et al.*, 2006; Wong *et al.*, 2010a). Additionally, a combination of difference satellite data was a good tool for air quality monitoring (Lee *et al.*, 2004b; Lee *et al.*, 2006a). As is difficult to quantify the environmental impacts of human and anthropogenic activities in urban areas, often many different indicators can conflict with each other. For examples, the positive relationship between the air quality and the UHI (Dwyer *et al.*, 1992; Klaus *et al.*, 1999), and its inverse relationship with biomass (Gallo *et al.*, 1993; Weng, 2001), surface temperature and UHI (Roth *et al.*, 1989; Nichol, 1994) are considered. In addition, the UEQ is an important factor for improving urban environment planning and management.

Previous studies referred show that urban quality can be estimated by the indices coupled with the socioeconomic and/or environmental data. Despite the benefits from previous studies, the scientific data for environmental assessment need to be tested as the indicator of urban quality. This study, therefore, presents a methodology for evaluating the UEQ parameters in an urban area using satellite remote sensing data in combination with ground based environmental measurements in GIS. The integration of various environmental parameters will provide a more detailed characterization of the state of urban environment than a single index approach.

2. Study area and dataset

A study area of approximately 3,318 km^2 (37° 46′ ~37° 20′ N, 126° 33′ ~127° 22′ E) which includes Seoul metropolitan area was chosen as shown in Fig. 1. Seoul is the largest city in Korea that covers an area of 607 km^2 and had a population of 9.747 millions. The city is surrounded by mountains and the Han River flows through the central part of the city. Because of high population density and anthropogenic activities, the UHI intensity in Seoul is significantly higher than any other cities in Korea. Kim and Baik (2004) reported that the average annual daily maximum UHI intensity in Seoul over the 29-year period (1971-2000) is 3.34° C. Seoul is divided into 25 *gu* (administrative unit of urban districts), where an automatic weather station (AWS) and an air quality measurement station were installed. Because this study requires the knowledge of the physical parameters of the meteorological and air quality

Table 1. Datasets used in this study.

Data	Index	Purpose
Landsat-7 ETM	Sep. 4, 2000 (UTC 0201) Sep. 23, 2001 (UTC 0159) Sep. 10, 2002 (UTC 0159)	Land cover, NDVI, Surface Temperature, Aerosol Reflectance, AOT,
Landsat-5 TM	Sep. 13, 2006 (UTC 0204)	Land cover, NDVI, Surface Temperature, Aerosol Reflectance, AOT
Ground-based	AWS, Air quality	Air Temperature, PM_{10}
GIS	Digital map, Admin. Boundary, Major road	Topography

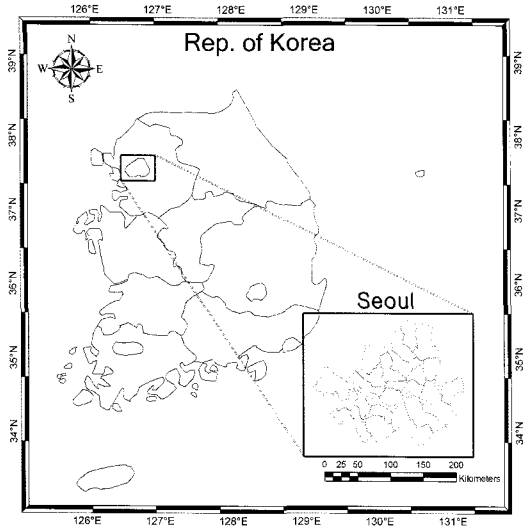

Fig. 1. Geographic boundary of this study.

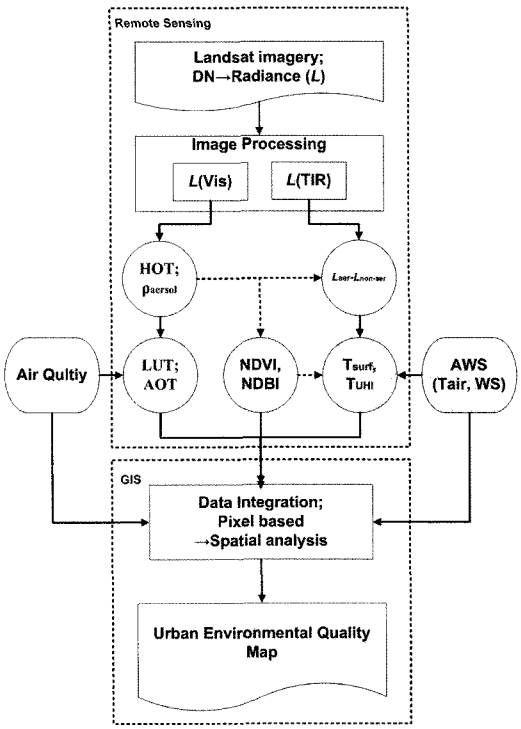

Fig. 2. Illustrative flow chart for the UEQ used in this study.

conditions, ground meteorological data and air quality data were also collected.

Fig. 2 illustrates the data processing for the UEQ evaluation adopted in this study. At the first step, the Digital Number (DN) values of Landsat image are converted into radiances (L) at each band using converting equation (Chander and Markham, 2003). One Landsat-5 TM and three Landsat-7 ETM+ images for which the spatial resolutions of visible and thermal infrared (TIR) bands are used in this study. Table 1 lists the acquisition dates and times of the Landsat images. The ETM data are observed at 0201 UTC on Sep. 4, 2000, 0159 UTC on Sep. 23, 2001, 0159 UTC on September 10, 2002, and TM data 0204 UTC on Sep. 13, 2006, respectively. All Landsat images were obtained within the same month under clear sky conditions for comparison purpose. Geometric correction to the study area was performed for the TM and ETM images using a third-order, cubic polynomial regression equation derived from twenty four Ground Control Points (GCP). Then

various environmental parameters including air quality, greenery, and UHI are derived from 30m spatial resolution Landsat images under clear sky condition while two ground based measurements including air quality monitoring and weather data are also implemented for supporting data. Finally, pixel-base satellite derived parameters are integrated in GIS for spatially assessing the UEQ. More detailed procedures and discussions for each step are following.

3. Air pollution retrieval from satellite

As most of the urban areas have high concentrations of air pollutants, the air quality in Seoul suffered for few decades. The pollution levels are often above air quality standards (AQS) and therefore it would be an important parameter for UEQ assessment. Although Landsat is not able to directly measure air quality, an approach for estimating Aerosol Optical Thickness (AOT) from Landsat spectral radiances is proposed here. AOT is a measure of the extent to which small particles in the atmosphere affect the transmission of sunlight through the atmosphere. The larger the AOT, the less sunlight reaches Earth's surface. A typical AOT value is roughly < 0.1 for clear sky condition and > 0.3 for hazy sky. Moreover, air pollution data from the ground based air quality monitoring stations such as PM_{10}, SO_2, NO_2, O_3, and CO concentrations are also implemented for estimating air quality conditions.

Precise retrieval of AOT from Landsat observation is more difficult than that from typical earth observing satellites such as AVHRR (Rao *et al.*, 1989), SeaWiFS (Gordon and Wang, 1994; Lee *et al.*, 2004a), MISR (Diner *et al.*, 1998), MODIS (Remer *et al.*, 2006; Lee *et al.*, 2007; 2008; Wong *et al.*, 2010b), HYPERION (Lee *et al.*, 2006b), and

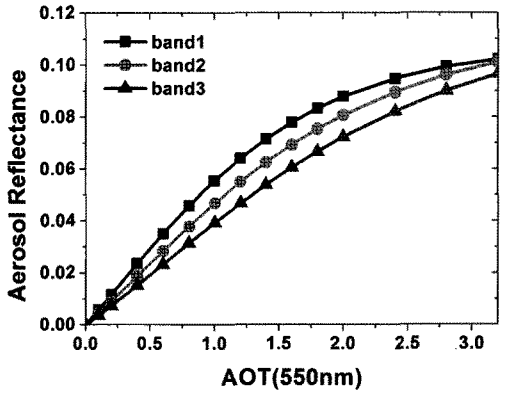

(a)

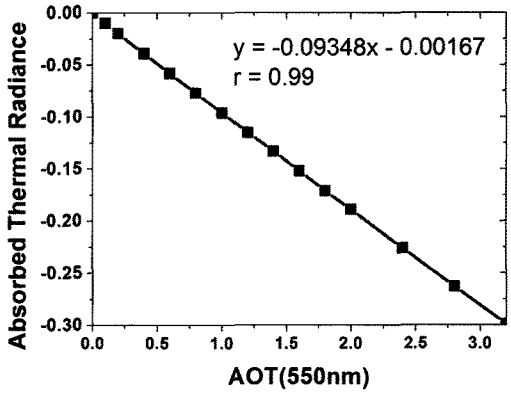

(b)

Fig. 3. Look-up tables for (a) AOT retrieval and (b) thermal radiation correction used in this study. Note that input data for the radiative transfer model are continental polluted aerosol model from OPAC (Hess *et al.*, 1998), solar zenith angle=48.6°, satellite viewing angle=0°, and azimuth angle=141.4°, respectively.

CHRIS (Wong *et al.*, 2010c). Because of complex surface reflectance and limited spectral information, large uncertainty exists in radiative transfer calculation for aerosol retrieval. Instead of direct radiative transfer scheme for traditional aerosol retrieval, in this study, the aerosol reflectance obtained from the Haze Optimized Transform (HOT) method (Zhang *et al.*, 2002; Zhang and Guindon, 2003; Dal Morro and Halounova, 2007) was employed to separate aerosol contributed radiance from Landsat radiances. The HOT method is relatively practical, scene-based simple technique and this approach involves isolating the aerosol

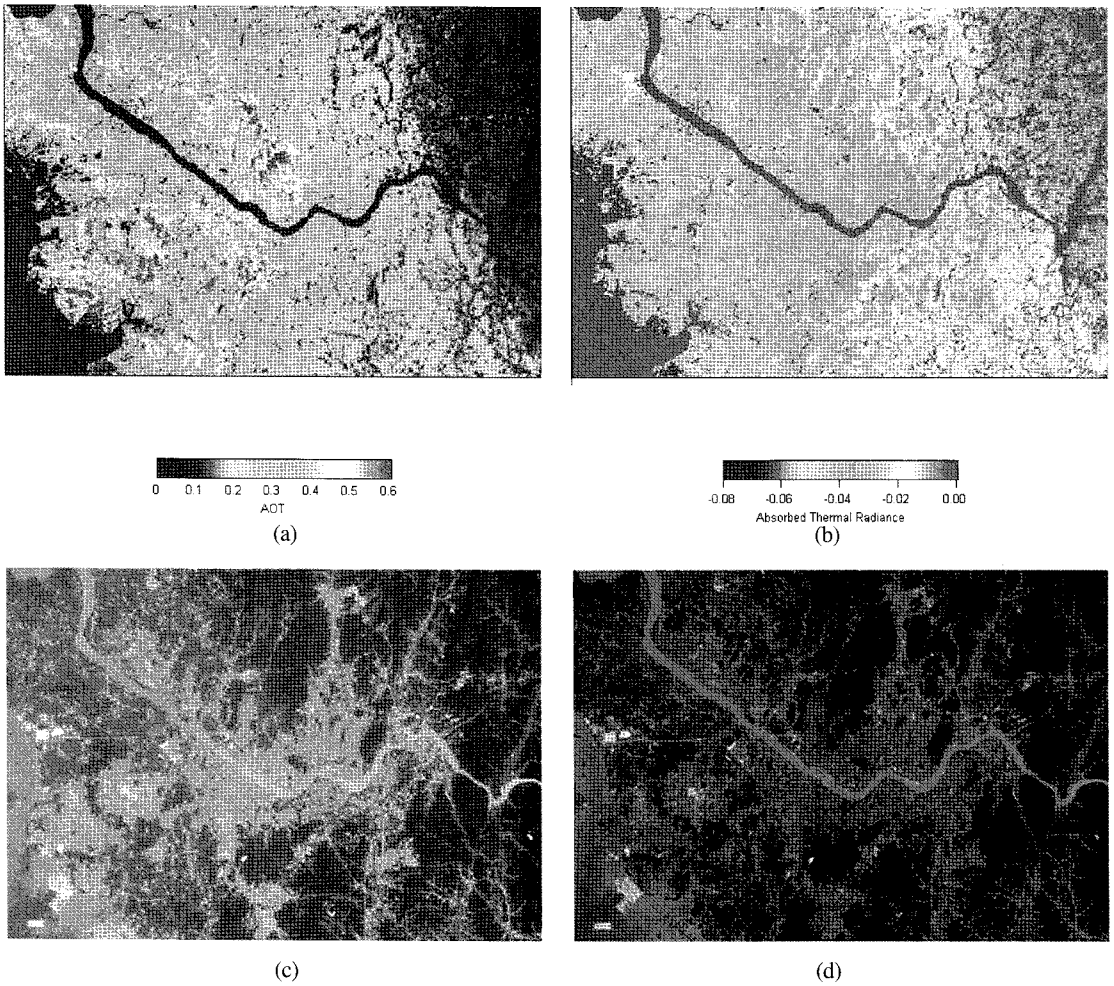

Fig. 4. AOT (scaled between 0 to 0.6) at 0.55um based on HOT (a), aerosol absorbed thermal radiance (scaled between -0.08 to 0) (b), Landsat RGB composite image before correction (c), and aerosol corrected image (d), respectively. Note that the color scale range for RGB image is 0~0.2 as visible band reflectances.

contribution in a scene through a radiometric transformation. The aerosol reflectance after the HOT process could convert into AOT using pre-calculated Look-Up Table (LUT) approach. LUT generated by radiative transfer modeling (Ricchiazzi *et al.*, 1998) includes satellite receiving radiance, reflectance, and transmittance at the surface level with various sun and viewing geometries. Input conditions for radiative transfer model used continental polluted aerosol model, dark surface, and AOT ranging from 0 to 3.

Fig. 3(a) shows the dependence of calculated aerosol reflectance as a function of AOT. The aerosol reflectances determined from the HOT process are able to convert to AOT using this relationship. Aerosol absorbing thermal radiance is also plotted in Fig. 3(b). Obviously, aerosols in the atmosphere can be absorbed by thermal radiation and the relation is linearly correlated. These are useful information for correcting aerosol absorption in thermal image interpretation in the section 4.

Fig. 4 shows the results for aerosol detection,

retrieval, and atmospheric correction for hazy Landsat images on Sep. 10, 2002. Among Landsat images used in this study, this image shows hazy as shown in Fig. 4(c). During the first step, Rayleigh scattering has been corrected according to the pixel based Rayleigh scattering calculation procedure (Lee *et al.*, 2006). In this step, Rayleigh path reflectance was determined from atmospheric pressure corrected scattering parameter obtained from the table of Bucholtz (1995). The height z km at a given pixel from The 30 meter resolution Advanced Spaceborne Thermal Emission and Reflection Radiometer (ASTER) Global Digital Elevation Model (GDEM) was used to calculate the atmospheric pressure determined by the following parameterized barometric equation.

$$P(z) = P_0 \cdot \exp\left[\frac{-29.87 \cdot g \cdot 0.75 \cdot z}{8.315 \cdot (T_{surf} - g \cdot 0.75 \cdot z)}\right] \quad (1)$$

Where, g is the gravity acceleration (9.807 m/s^2), is altitude above sea level in km, T_{SURF} is surface temperature which was assumed as 298° K. Then the Rayleigh path reflectance can be determined with this pressure at each wavelength in each pixel.

Without the Rayleigh scattering correction, high reflection by air molecules in shorter wavelength can make the blue color/wavelength brighter. Then HOT is performed to separate aerosol contribution in this Rayleigh scattering corrected image. This result in fine resolution and discrete pattern shows a lot of pixels with missing values because HOT process is not performed for water and highly bright pixel (Zhang *et al.*, 2002). Thus, the missing values were filled with neighboring pixels and then applied a Gaussian Kernel convolution on the images. However, pixels for ocean and in-land water were excluded in this step. The size of Gaussian filter was selected to be 150m × 150m (5 × 5) pixel. Fig. 4(b) shows the aerosol absorbed thermal radiance. Heavy aerosol region (AOT > 0.3) shows more absorbing thermal radiances lager than 0.03 W/m^2/sr. Additionally, Landsat RGB images of before- and after-correction are also shown in Fig. 4(c) and (d).

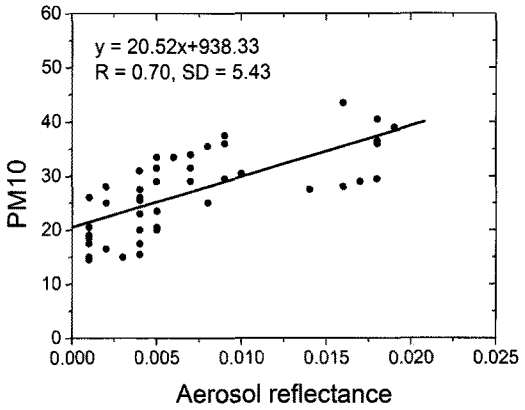

Fig. 5. Comparison between the Landsat derived aerosol reflectance (ρ_a) and PM_{10} mass concentrations in $\mu g/m^3$.

For the robust estimation about whether the AOT from Landsat data are related with air quality or not, retrieved AOT values were compared with ground-based PM_{10} concentration data. Obviously there exists difference between two parameters. PM_{10} is ground level aerosol mass concentration while AOT is a column integrated radiation. In spite of this difference, the comparison of Landsat AOT versus PM_{10} shows good correlations as shown in Fig. 5. This means Landsat AOT is useful to UEQ estimation as a parameter of the spatial distribution of atmospheric aerosols over study area.

4. Surface temperature

The spatial and temporal distribution of the temperature is a fundamental parameter of urban environment since it is sensible by human (human comfort). In order to estimate spatial temperature distribution, 60m resolution ETM+ TIR (thermal infrared) band radiance was converted into the

brightness temperature T_b (°K) using the following equation (Wukelic *et al.*, 1989).

$$T_b = \frac{K_2}{\ln\left(\frac{K_1}{L}\right) + 1} \quad (2)$$

where, K_1, K_2 are calibration constant form Landsat conversion table in W/m^2 · sr · mm. L is atmospherically corrected thermal radiance. Satellite data were also re-sampled to 30m resolution in order to allow proper registration of TIR with other 30m VIS bands.

Based on the maximum likelihood classification method, land cover classification was also performed in this step. Spectral reflectance at seven bands and the NDVI are involved for land cover classification. The training areas were selected on those invariant-pseudo targets and five classifiers were determined, which are water, urban, grass, tree, and soil, respectively. The classified images are then used to make an emissivity image using the specific emissivity (ε) of water (0.99), forest (0.974), grassland (0.91), urban (0.92) and soil (0.95) (Nichol, 1994; 1996). At the same time the emissivity corrected surface temperature (T_s) from the thermal image is corrected using the Planck's constant for differences in emissivity among each land cover type (Artis and Carnahan, 1982):

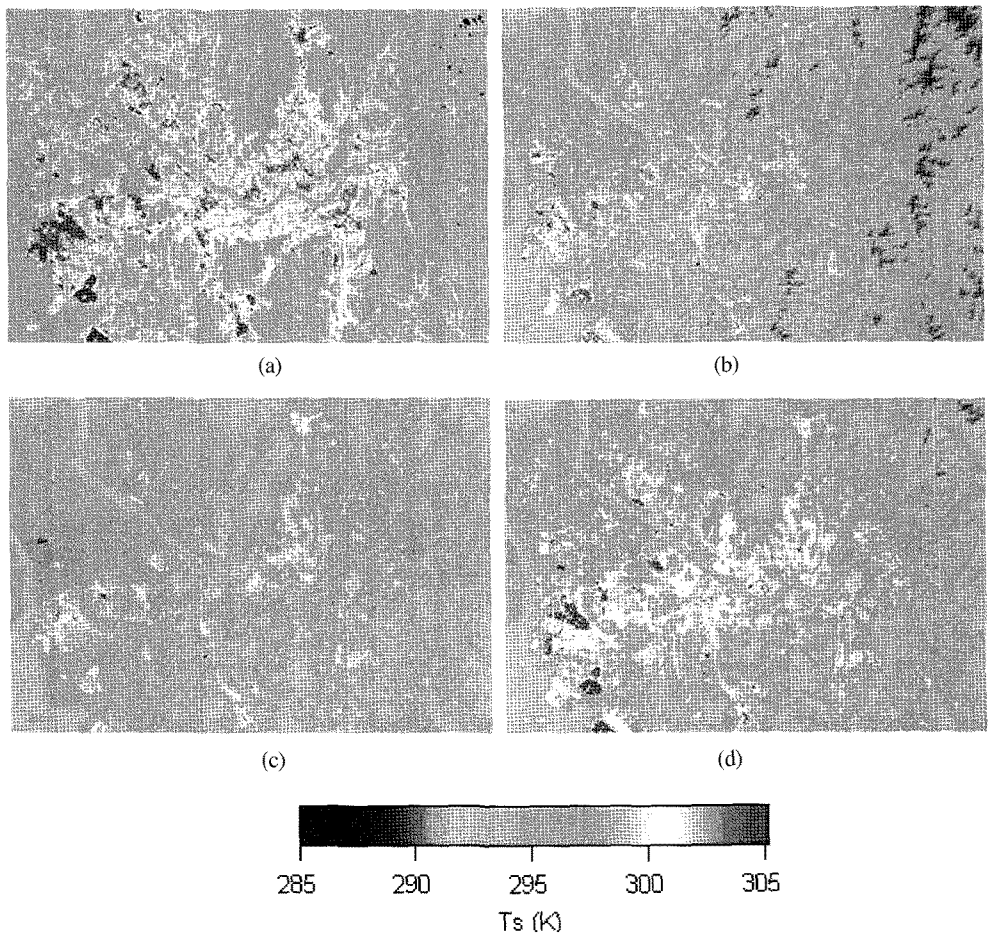

Fig. 6. Surface temperature distribution in Seoul metropolitan area, Korea on (a) Sep. 4, 2000, (b) Sep. 23, 2001, (c) Sep. 10, 2002, and (d) Sep. 13, 2006, respectively.

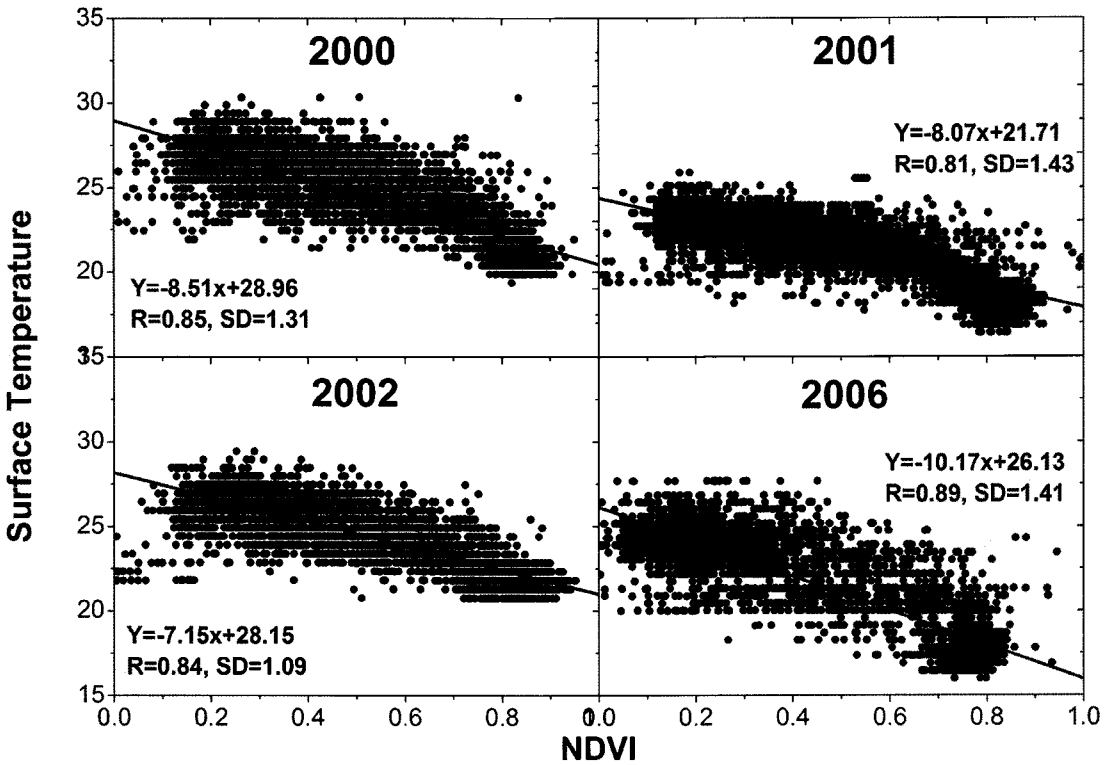

Fig. 7. Correlation between NDVI with surface temperature (*Ts*).

$$T_S = \frac{T_b}{1 + (\lambda T_b/\alpha) \cdot \ln \varepsilon} \quad (3)$$

where λ = wavelength of emitted radiance, T_b = Brightness temperature (° K), $\alpha = hc/K$ (1.438×10^{-2} m° K), h = Planck's constant (6.62×10^{-34} J · sec), c = velocity of light (2.998×10^{8} m/sec), and K = Stefan Bolzmann's Constant (1.38×10^{-23} J/° K), respectively.

Fig. 6 shows the Landsat derived *Ts* distribution for all cases. Although the range of temperatures is narrow for each image except for the case of year 2000, the surface temperatures of the urbanized areas are always higher than those of the rural areas. The general temperature differences between urban and rural area (T_{urban}-T_{rural}) were 8.45° K (2000), 9.14° K (2001), 8.61° K (2002), and 8.41° K (2006), respectively. Although the UHI values are similar during these years, the spatial coverage of "hot" surface temperature (> 297° K) significantly increased from year 2001 to 2006 due to the rapid urban development. The 2000 case shows higher values than others because of higher solar insolation in the end of summer.

The *Ts* highly depends on land cover type because of the emissivity of surface objects. Generally green area has lower values than urban area. Fig. 7 shows this relationship very well. The linear regressions between the *Ts* and NDVI are highly correlated. Correlation coefficients were observed as 0.85 (2000), 0.81 (2001), 0.84 (2002), and 0.89 (2006), respectively. This suggests that the dense vegetation can cool down the surface temperature and planting inside the metropolitan areas is important for mitigating the effect of UHI.

Table 2 summarizes the mean and standard

Table 2. Statistics of surface temperature (Ts) for different land cover types.

Land cover	Sep. 4, 2000			Sep. 23, 2001			Sep. 10, 2002			Sep. 13, 2006		
	m	σ	n	m	σ	n	m	σ	n	m	σ	n
Urban	27.8	0.9	301343	24.4	0.9	268343	24.7	0.9	196599	25.9	1.3	182406
Grass	22.5	0.5	127379	20.6	0.6	209711	19.8	0.3	204052	22.6	1.8	254817
Tree	20.9	0.9	409805	16.6	1.2	335456	19.0	0.8	347196	18.3	1.2	303117
Soil	27.2	2.4	50757	26.1	2.1	62240	24.9	1.4	145881	24.0	3.8	151749
water	21.1	1.1	70566	18.9	0.7	65600	18.5	0.8	66122	19.6	1.4	67761

m: mean, σ: standard deviations, n: number of pixels

Table 3. Index level of four UEQ parameters to determine UEQ index refered in Eq (4).

Index Level	1(very bad)	2(bad)	3(sensible)	4(moderate)	5(good)	6(very good)
Ts [°C]	>35	30-35	28-30	26-28	24-26	< 24
ρa	>0.04	0.035-0.04	0.030-0.035	0.015-0.030	0.01-0.015	<0.01
PM_{10}[$\mu g/m^3$]	>300	200-300	150-200	100-150	50-100	<50
NDVI	<0.5	0.6-0.65	0.65-0.7	0.7-0.75	0.75-0.8	>0.8

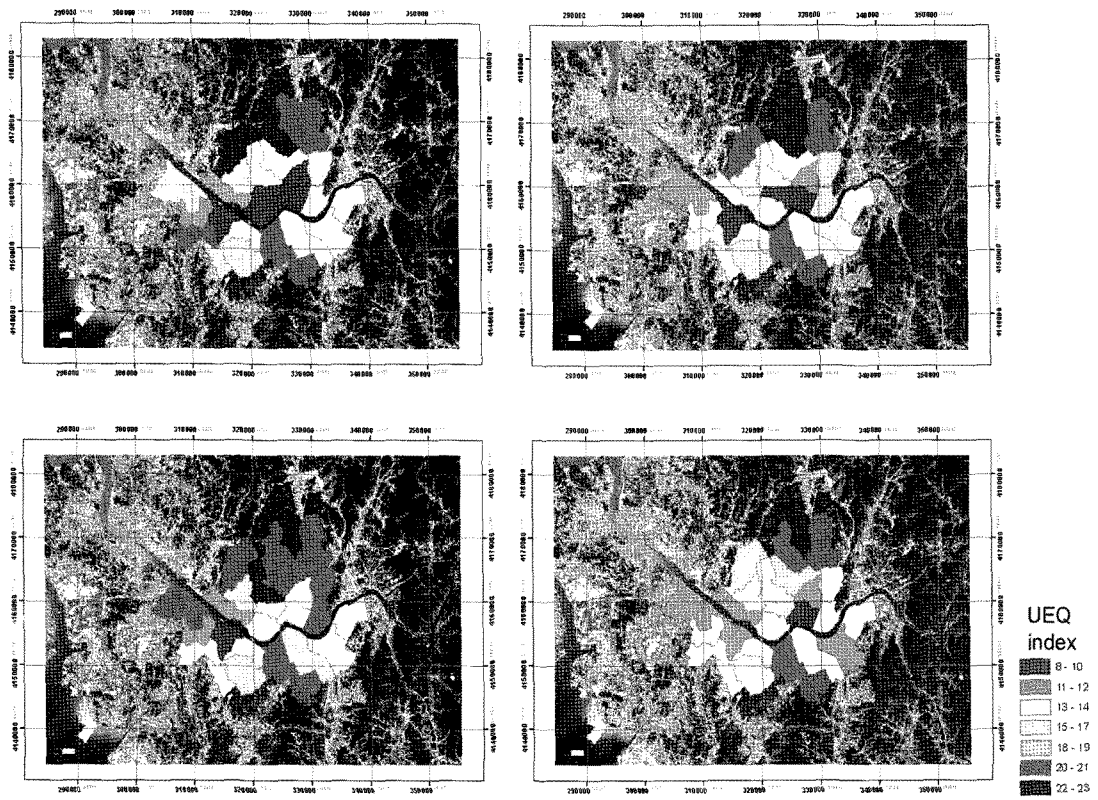

Fig. 8. UEQ index maps for Seoul, Korea, in (a) year 2000, (b) 2001, (c) 2002, and (d) 2006, respectively.

deviations of *Ts* for each land cover type for the five classes. The tree (or forest) has the lowest surface temperature where urban and soil has the highest. It was true in most part of the mega cities the highest

surface temperature due to high albedo object such as concrete and soil appears around the year. Thus, suggestions like more vegetation planting and more streams and rivers passing through the cities were adopted for reducing the UHI effect.

5. Urban environmental quality mapping

By combining the ground based AWS and air quality monitoring, and satellite derived data including surface temperature *Ts*, air temperature *Ta*, vegetation fraction NDVI, air quality (PM_{10}), aerosol reflectances ρa in a database, 6 different classes (from 1 to 6) were classified based on all five parameters (see Table 4). Then each index parameter was sumed to have a final UEQ index (UEQI) value.

$$UEQI = I(T_s) + I(T_a) + I(NDVI) + I(PM_{10}) + I(\rho a) \quad (4)$$

where w is the weighting factor for each parameter. Each administrative polygon represents one UEQI value. Fig. 8 illustrates the UEQI map from 2000 to 2006. It is surprising that two districts (*Seongdong gu and Yeongdeungpo gu*) are generally high UEQI value over this period. Also, it is indicated that the increases in air pollutant (PM_{10} and aerosol reflectance), reduction of vegetation areas (decreasing of NDVI) and increases in temperature induce the declining of UEQ (e.g. high UEQ class) over most of the districts from 2000 to 2006.

6. Summary and conclusion

Satellite remote sensing data enable to improve the understanding of relationships among topography, the UHI, greenness, and air pollution within an urban area which are complex delete and and dynamic and only superficially understood. This study made an advance over previous works (Nichol *et al*, 2005; 2006) to use a remote sensing data as an index of UEQ, which have used only a single separated parameter. The use of Landsat multispectral imagery with high spatial and radiometric resolution permits quantification of temperature, greenery, and air pollution at the detailed level of a city by the systematic process in the field of image analyses. This provides an opportunity to verify the feasibility of satellite remote sensing for estimation of the UEQ monitoring. The results are summarized as follows.

* Determinations of aerosol reflection and radiation correction were successfully carried out to Landsat imagery by the HOT process with LUT approach. Satellite derived aerosol property data are well matched with ground based aerosol concentrations. This suggests that satellite provides more compatible spatial resolution data for air pollutant mapping.
* The NDVI was used to estimate the fraction of green space in an urban area and examine the relation between thermal behavior and vegetation cover amount. Results show that the higher temperature over urban area was also confirmed by satellite measurement and is well correlated to NDVI.
* The combination of satellite- and ground-based data provides an integrated UEQI which can represent the detailed spatial variations and thus comparisons between individual urban administration units. The UEQI map by GIS was also analyzed for the 25 urban districts in Seoul, Korea. The district areas of lower UEQI were identified in this study as being low vegetation fraction, high air pollution, high surface and air temperature. In order to increase the UEQ in this area watering to promote cooling by evapo-transpiration, as well as the addition of vegetated sections and road cleaning for controlling of

particles are recommended.

Although this work is limited to medium-resolution sensors from Landsat ETM and TM, the use of higher spatio-temporal resolution images from other satellites observation will give more detailed quantification of the UEQ.

Acknowledgements

This work was supported by the Mid-career Researcher Program through the National Research Foundation of Korea (NRF) grant funded by the Korea government (MEST) (No. 2010-0025871). The research from M. S. Wong was supported by Hong Kong Public Policy Research Project PPR-K-QZ04 and PolyU PDF Research Grant G-YX1W. The research from Y. J. Kim was supported by the NRF grant funded by the MEST (No. 2008-0060618) and the Korea Meteorological Administration Research and Development Program under Grant RACS_2010-1002.

References

Artis, D. A. and W. H. Carnahan, 1982. Survey of emissivity variability in thermography of urban areas, *Remote Sensing of the Environment*, 12: 313-329.

Bucholtz, A., 1995. Rayleigh-scattering calculations for the terrestrial atmosphere, *Appl. Optics*, 34: 2765-2773.

Chander, G. and B. Markham, 2003. Revised Landsat-5 TM Radiometric Calibration Procedures and Post-calibration Dynamic Ranges, *IEEE Transactions on Geoscience and Remote Sensing*, 41(11): 2674-2677.

Dal Moro, G. and L. Halounova, 2007. Haze removal for high-resolution satellite data: A case study, *International Journal of Remote Sensing*, 28(10): 2187-2205.

Diner, D., J. Beckert, T. H. Reilly, C. Bruegge, J. E. Conel, R. A. Kahn, J. Matonchik, T. P. Ackerman, R. Davies, S. A. W. Gerstl, H. Gordon, J. P. Muller, R. B. Myneni, P. J. Sellers, B. Pinty, and M. M. Verstraete, 1998. Multi-angle Imaging SpectroRadiometer (MISR) instrument description and experiment overview, *IEEE Transactions on Geosciences and Remote Sensing*, 36(4): 1072?1087.

Dwyer, J. F., G. E. Macpherson, H. W. Schoeder, and R. A. Rowntree, 1992. Assessing the benefits and costs of the urban forest, *Journal of Arboriculture*, 18(5): 227-234.

Forster, B., 1983. Some urban measurements from Landsat data, *Photogrammetric Engineering and Remote Sensing*, 49(12): 1693-1707.

Gallo, K. P., A. L. Mcnab, T. R. Karl, J. F. Brown, J. J. Hood, and J. D. Tarpley, 1993. The use of NOAA AVHRR data for assessment of the urban heat island effect, *Journal of Applied Meteorology*, 32: 899-908.

Gordon, H. R. and M. Wang, 1994. Retrieval of water-leaving radiance and aerosol optical thickness over the oceans with SeaWiFS: preliminary algorithm, *Applied Optics*, 33(3): 443-452.

Hess, M., P. Koepke, and I. Schult, 1998. *Optical Properties of Aerosols and clouds: The software package OPAC*, Bull. Am. Met. Soc., 79: 831-844.

Kim, Y. H. and J. J. Baik, 2004. Daily maximum urban heat island intensity in large cities of Korea, *Theor. Appl.* Climatol., 79: 151-164.

Klaus, D., E. Jauregui, A. Poth, G. Stein, and M. Voss, 1999. Regular circulation structures in the tropical basin of Mexico City as a

consequence of the heat island effect, *Erdkunde*, 53: 231-243.

Lee, D. H., K. H. Lee, and Y. J. Kim, 2006a. Application of MODIS aerosol data for aerosol type classification, *Korean J. of Remote Sensing*, 22(6): 495-505.

Lee, D. H., K. H. Lee, and Y. J. Kim, 2006b. Atmospheric aerosol detection and its removal for satellite data, *Korean J. of Remote Sensing*, 22(5): 1-5.

Lee, K. H., Y. J. Kim, and W. von Hoyningen-huene, 2004a. Estimation of aerosol optical thickness over Northeast Asia from SeaWiFS data during the 2001 ACE-Asia IOP, *Journal of Geophysical Research*, 109, D19S16.

Lee, K. H., C. S. Hong, and Y. J. Kim, 2004b. Atmospheric aerosol monitoring over northeast Asia during 2001 from MODIS and TOMS data, *Korean J. of Remote Sensing*, 20(2): 77-89.

Lee, K. H., Y. J. Kim, J. Kim, W. von Hoyningen-huene, and J. P. Burrow, 2006. Influence of land surface effects on MODIS aerosol retrieval using the BAER method over Korea, *International Journal of Remote Sensing*, 27(14): 2813-2830.

Lee, K. H., L. Zhanqing, and Y. J. Kim, 2007. SWIR/VIS reflectance ratio over Korea for aerosol retrieval, *Korean J. of Remote Sensing*, 23(1): 1-5.

Lee, K. H. and Y. J. Kim, 2008. Difference between collection4 and 5 MODIS aerosol products and comparison with ground based measurements, *Korean J. of Remote Sensing*, 24(4): 369-379.

Lo, C. P. and B. J. Faber, 1997. Integration of Landsat thematic mapper and census data for quality of life assessment, *Remote Sensing of Environment*, 62: 143-157.

Nichol, J. E., 1994. A GIS-based approach to microclimate monitoring in Singapore's high rise housing estates, *Photogrammetric Engineering and Remote Sensing*, 60: 1225-1232.

Nichol, J. E., 1996. Analysis of the urban thermal environment with LANDSAT data, *Environmental Planning B: Planning and Design*, 23: 733-747.

Nichol, J. E. and M. S. Wong, 2005. Modeling urban environmental quality in a tropical city, *Landscape and Urban Planning*, 73: 49-58.

Nichol, J. E., M. S. Wong, C. Fung, and K. K. M. Leung, 2006. Assessment of urban environmental quality in a subtropical city using multispectral satellite images, *Environmental Planning B: Planning and Design*, 33(1): 39-58.

Rao, N. C. R., L. L. Stowe, and E. P. Mcclain, 1989. Remote sensing of aerosols over oceans from AVHRR, *International Journal of Remote Sensing*, 10(4-5): 743-749.

Remer, L., D. Tanre, and Y. Kaufman, 2006. Algorithm for Remote Sensing of Tropospheric Aerosols from MODIS: Collection 5, Algorithm Theoretical Basis Document, *http://modis.gsfc.nasa.5gov/data/atbd/atmosatbd.php*.

Ricchiazzi, P., S. Yang, C. Gautier, and D. Sowle, 1998. SBDART: A research and teaching software tool for plane-parallel radiative transfer in the Earth's atmosphere, *Bulletin of the American Meteorology Society*, 79(10): 2101-2114.

Roth, M., T. R. Oke, and W. J. Emery, 1989. Satellite derived urban heat islands from three coastal cities and the utilisation of such data in urban climatology, *International Journal of Remote Sensing*, 10(11): 1699-1720.

Stathopoulou, M. and C. Cartalis, 2007. Daytime urban heat island from Landsat ETM+ and Corine land cover data: An application to

major cities in Greece, *Solar Energy*, 81: 358-368.

Voogt, J. A. and T. R. Oke, 2003. Thermal remote sensing of urban climates, *Remote Sensing of Environment*, 86(3): 370-384.

Weber, C. and J. Hirsch, 1992. Some urban measurements from SPOT data: urban life quality indices, *International Journal of Remote Sensing*, 13(17): 3251-3261.

Weng, Q., 2001. A remote sensing-GIS evaluation of urban expansion and its impact on surface temperature in the Zhujiang Delta, China, *International Journal of Remote Sensing*, 22(10): 1999-2014.

Wong, M. S., J. E. Nichol, and K. H. Lee, 2010a. A satellite view of urban heat island: cuaseative factors and scenario analysis, *Korean J. of Remote Sensing*, 26(6): 617-627.

Wong, M. S., K. H. Lee, J. E. Nichol, and Z. Li, 2010b. Retrieval of Aerosol Optical Thickness using MODIS $500 \times 500m^2$, a study in Hong Kong and Pearl River Delta region, *IEEE Transaction of Geoscience and Remote Sensing*, 48(8): 3318-3327.

Wong, M. S., K. H. Lee, and J. E. Nichol, 2010c. Aerosol optical thickness retrieval using a small satellite, *Korean J. of Remote Sensing*, 26(6): 605-615.

Wukelic, G. E., D. E. Gibbons, L. M. Martucci, and H. P. Foote, 1989. Radiometric calibration of Landsat thematic mapper thermal band, *Remote Sensing of Environment*, 28: 339-347.

Zhang, Y., B. Guindon, and J. Cihlar, 2002. An image transform to characterize and compensate for spatial variations in thin cloud contamination of Landsat images, *Remote Sensing of Environment*, 82: 173-187.

Zhang, Y. and B. Guidon, 2003. Quantitative assessment of a haze suppression methodology for satellite Imagery: effect on land cover classification performance, *IEEE Transactions on Geoscience and Remote Sensing*, 41: 1082-1089.